

## The Effect of Discharge Depth on Contaminant Dispersion in Turbulent Open Channel Flow

*Albert J. Gabric*

Centre for Environmental Studies, University of Melbourne, Parkville, Vic. 3052;  
present address: Control Data Australia, 493 St. Kilda Road, Melbourne, Vic. 3004.

### *Abstract*

The transport and diffusion of neutrally buoyant, conservative contaminants in an open, finite depth channel is analysed at times before uniform mixing over the depth has occurred. Analytical expressions for the total mass at a given depth, the centre of mass and the variance of the contaminant patch are presented.

### **1. Introduction**

The transport and diffusion of a contaminant in a shallow, wide open channel is analysed. The current field is horizontally uniform and any horizontal boundaries are far enough from the release position that the contaminant does not interact with the boundaries within the times considered. The flow may thus be considered two dimensional and such a model could be applied to estuaries or coastal waters with a well-defined current field and negligible secondary circulation. This is often the case when the predominant currents are tidally driven and the coastline or embayment geometry simple.

The vertical current profile is modelled by a power law variation. This formulation has been suggested as a good approximation to the actual shear distribution in a channel, and has the advantage of making the problem tractable analytically (Fukuoka 1973). In fact the power law has been shown to be a valid approximation for a wide range of naturally occurring boundary layer flows and also well represents the velocity in the region of the bottom boundary. The wall region of a boundary layer has been shown to be well described by Prandtl's 1/7th power law (Hinze 1959; Schubauer and Tchen 1961), although this law slightly overestimates the fluid velocity near the wall.

The vertical diffusivity profile is also assumed to vary according to a power law formula. Reynolds analogy is assumed to hold and this leads to a specific relationship between the exponents in the power laws for the velocity  $u(z)$  and the diffusivity  $K_{zz}(z)$ . As pointed out by Csanady (1973), the choice of a diffusivity profile amounts to a guess of the properties of the concentration field and may lead to erroneous conclusions. The final arbiter must be the model's ability to reproduce any existing experimental data; however the author feels that the choice of a power law is at least better than the constant velocity and diffusivity assumption.

Theoretical analyses of diffusion in an open channel have mainly extended the asymptotic treatment by Taylor (1953, 1954). Aris (1956) derived the same results

as Taylor in terms of the integral moments of the concentration distribution. Elder (1959) extended Taylor's work to turbulent flow and conducted a series of experiments on dye diffusion in a flume. Before the asymptotic stage had been reached, Elder observed a skewed longitudinal concentration distribution characterized by a long upstream tail. Elder attributed the formation of a tail to the retentive effects of the viscous sublayer, although no theoretical analysis was done (see Appendix).

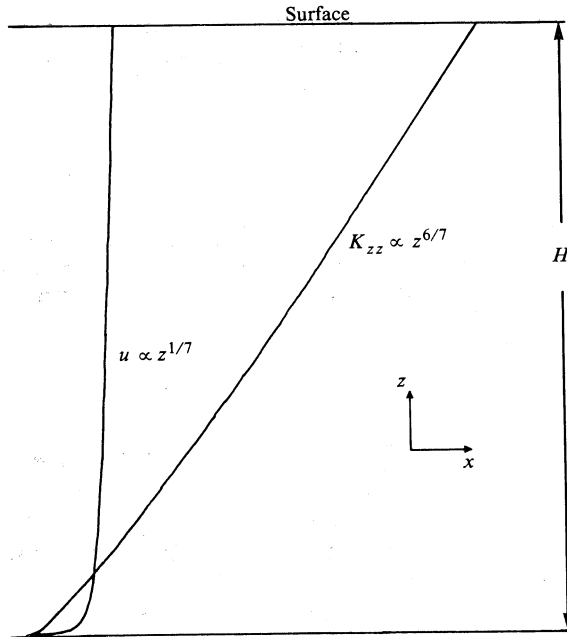


Fig. 1. Schematic representation of the velocity  $u$  and diffusivity  $K_{zz}$  profiles.

The reason for the skewness for small diffusion times may be intuitively understood from Fig. 1. After release the motion of a tracer patch is influenced by the velocity profile which is nearly uniform over most of the depth but has a large gradient near the bottom boundary. Consequently the tracer will develop a long tail as material is transported from the uniform velocity region towards the bottom. The time of onset of tail formation will depend on the release position and the rate of vertical transport. Eventually the longitudinal concentration distribution approaches the gaussian limit when the tracer is uniformly distributed over the depth. This approach to normality has been studied by Chatwin (1970) in an analysis of Poiseuille flow in a pipe.

The non-asymptotic stage of diffusion in a channel has not been treated analytically, with the exception of Okubo (1967) who considered a linear velocity profile and constant diffusivity. Experimental data on the non-asymptotic diffusion of dye in a flume has been gathered by Sullivan (1971); however, depth integrated concentrations were measured and thus no vertical concentration distribution was recorded, which is often of interest in environmental considerations. Sullivan identified three stages in the longitudinal diffusion process, depending on the degree of mixing over depth. The object of the present work is to obtain analytical expressions for the integral moments of the concentration distribution at times less than the vertical

mixing time. The vertical mixing time may be comparable to the tidal period in some instances; however, for simplicity, the current field is assumed to be steady in this analysis.

For non-asymptotic diffusion times, the vertical discharge location influences the pollutant concentration distribution downstream. Thus the depth positioning of a proposed outfall may be tested by the model. The results indicate that for a discharge position close to the bottom, almost the entire release mass will reside in the lower half of the channel for short diffusion times. This prediction must be related to the greater longitudinal spreading ability of the lower layer, and a trade-off between toxicity effects on the benthos in the vicinity of the outfall versus long-term contaminant dilution must be made in a particular case.

## 2. Moments of Concentration Distribution

In order to allow for an analytical treatment the following assumptions are made:

- (1) the flow is considered two dimensional and any horizontal variations are neglected;
- (2) the vertical velocity profile is well represented by a power law;
- (3) Reynolds analogy holds which implies a power law variation for the vertical diffusivity;
- (4) the tracer is released instantaneously at a point  $(0, z_0)$ ;
- (5) the depth of the channel is a constant.

The coordinate system is chosen so that the  $x$ -axis is parallel to the current, the  $y$ -axis across the current and the  $z$ -axis vertically upwards (see Fig. 1). If we ignore lateral diffusion, the convective-diffusion equation may be written

$$\frac{\partial c}{\partial t} + (az^m) \frac{\partial c}{\partial x} = K_{xx} \frac{\partial^2 c}{\partial x^2} + \frac{\partial}{\partial z} \left( K_{zz} \frac{\partial c}{\partial z} \right), \quad (1)$$

where  $a$  is a constant. The initial and boundary conditions are given by

$$c(x, z, t=0) = M \delta(x) \delta(z-z_0), \quad (2a)$$

$$K_{zz} \partial c / \partial z = 0, \quad \text{at } z = 0 \text{ and } H, \quad (2b)$$

$$c(x, z, t) \rightarrow 0, \quad \text{as } x \text{ tends to infinity}, \quad (2c)$$

where  $H$  is the channel depth (see Fig. 1) and  $M$  the release mass. If Reynolds analogy is applicable then  $K_{zz} = T(du/dz)^{-1}$ , where  $T$  is the kinematic shear stress. In an open channel flow driven by a constant pressure gradient, the shear stress is given by (Fukuoka 1973)  $T = u^{*2}(1 - z/H)$ , where  $u^*$  is the frictional velocity. This leads to  $K_{zz} = bz^{1-m}(1 - z/H)$ ; however, since the velocity shear is greatest near the channel bed (Fig. 1), it is reasonable to assume that

$$K_{zz} = bz^{1-m}, \quad b = u^{*2}/ma, \quad \text{where } 0 < m < 1. \quad (3a, b)$$

Equation (1) proves to be too formidable for a direct analytical solution but it is possible to derive from it more manageable equations for the moments of the concentration distribution using the method of Aris (1956). The  $p$ th moment of the concentration distribution at a depth  $z$  and time  $t$  is defined by

$$\Theta_p(z, t) = \int_{-\infty}^{\infty} x^p c(x, z, t) dx, \quad (4)$$

with  $p = 0, 1, 2, \dots$ . Integrating equation (1) over  $x$  and applying the boundary condition (2c) gives

$$\frac{\partial \Theta_0}{\partial t} = \frac{\partial}{\partial z} \left( K_{zz} \frac{\partial \Theta_0}{\partial z} \right), \quad (5)$$

where  $\Theta_0(z, t)$  the zeroth moment is the total amount of material that has reached a given depth  $z$  after time  $t$ . As was pointed out by Saffman (1962),  $\Theta_0$  is independent of the current profile  $u(z)$  since, although the distortion of the patch by the shear increases for vertical concentration gradients, it does so for both positive and negative gradients. Thus, there is no net effect on total vertical transport of material. The associated boundary conditions are given by

$$\Theta_0(z, t=0) = M \delta(z-z_0); \quad K_{zz} \partial \Theta_0 / \partial z = 0, \quad \text{at } z = 0 \text{ and } H. \quad (6a, b)$$

Multiplying equation (1) by  $x$  and integrating gives

$$\frac{\partial \Theta_1}{\partial t} - \frac{\partial}{\partial z} \left( K_{zz} \frac{\partial \Theta_1}{\partial z} \right) = u(z) \Theta_0(z, t), \quad (7)$$

where the first moment defines the centroid of a patch slice by the relation

$$\bar{x}(z, t) = \Theta_1(z, t) / \Theta_0(z, t). \quad (8)$$

Equation (7) must be solved subject to the initial and boundary conditions

$$\Theta_1(z, t=0) = 0, \quad K_{zz} \partial \Theta_1 / \partial z = 0, \quad \text{at } z = 0 \text{ and } H. \quad (9a, b)$$

Multiplying equation (1) by  $x^2$ , integrating and applying the boundary conditions gives the equation for the second moment

$$\frac{\partial \Theta_2}{\partial t} - \frac{\partial}{\partial z} \left( K_{zz} \frac{\partial \Theta_2}{\partial z} \right) = 2K_{xx} \Theta_0 + 2u(z) \Theta_1, \quad (10)$$

which must be solved subject to conditions analogous to equations (9). Similarly, the equations for the higher order moments may be derived if required. The variance of the patch slice at depth  $z$  and time  $t$  is given by

$$\sigma_x^2(z, t) = \Theta_2(z, t) / \Theta_0(z, t) - \{\Theta_1(z, t) / \Theta_0(z, t)\}^2. \quad (11)$$

Alternatively, a less detailed treatment of the patch statistics may be carried out by defining the depth integrated moments

$$\Phi_p(t) = \int_0^H \Theta_p(z, t) dz. \quad (12)$$

Then the centroid of the entire patch is given by

$$\bar{x}(t) = \Phi_1 / M, \quad (13)$$

where  $\Phi_1$  is obtained by integrating equation (7) over the depth. The variance of the entire patch is defined by

$$\Sigma_x^2(t) = (\Phi_2 / M) - (\Phi_1 / M)^2, \quad (14)$$

and  $\Phi_2$  is obtained by integrating equation (10) over the depth.

### 3. Solution for Zeroth Moment

The Laplace transform of  $\Theta_0(z, t)$  is defined as

$$\tilde{\Theta}_0(z, w) = \int_0^\infty \Theta_0(z, t) \exp(-wt) dt. \quad (15)$$

Multiplying equation (5) by  $\exp(-wt)$ , integrating and applying the initial condition gives

$$\frac{d}{dz} \left( K_{zz} \frac{d\tilde{\Theta}_0}{dz} \right) - w\tilde{\Theta}_0 = -M \delta(z - z_0). \quad (16)$$

This non-homogeneous equation can be written in an equivalent form that does not involve the delta function (Stakgold 1968). Thus, we have

$$\frac{d}{dz} \left( K_{zz} \frac{d\tilde{\Theta}_0}{dz} \right) - w\tilde{\Theta}_0 = 0, \quad \text{for } 0 < z < z_0 \text{ and } z_0 < z < H, \quad (17a)$$

$$\tilde{\Theta}_0(z = z_0+) = \tilde{\Theta}_0(z = z_0-), \quad (17b)$$

$$\left. \frac{d\tilde{\Theta}_0}{dz} \right|_{z=z_0+} - \left. \frac{d\tilde{\Theta}_0}{dz} \right|_{z=z_0-} = -\frac{M}{K_{zz}(z_0)}, \quad (17c)$$

where equation (17b) represents the continuity requirement on  $\tilde{\Theta}_0$  at  $z = z_0$ , and (17c) gives the jump condition that must be satisfied by the derivatives of  $\tilde{\Theta}_0$ .

Substituting for  $K_{zz}(z)$  in equation (17a) and simplifying gives

$$z^2 \frac{d^2 \tilde{\Theta}_0}{dz^2} + (1-m)z \frac{d\tilde{\Theta}_0}{dz} - \frac{w}{b} z^{1+m} \tilde{\Theta}_0 = 0. \quad (18)$$

By comparison with Bessel's equation the general solution of (18) may be written as

$$\tilde{\Theta}_0(z, w) = Az^{\frac{1}{2}m} I_\nu(\phi) + Bz^{\frac{1}{2}m} I_{-\nu}(\phi), \quad (19)$$

where  $A$  and  $B$  are constants to be derived by application of the boundary conditions

$$\nu = m/(1+m), \quad \phi = (w/b)^{\frac{1}{2}} 2z^{\frac{1}{2}(1+m)}/(1+m) = kw^{\frac{1}{2}}, \quad (20a, b)$$

and  $I_\nu$  denotes the modified Bessel function of the first kind of order  $\nu$ . From equations (20a) and (3a) the value of  $\nu$  is in the range  $0 < \nu < \frac{1}{2}$ .

The solution given in equation (19) must satisfy the boundary conditions

$$K_{zz}(z) \partial \tilde{\Theta}_0 / \partial z = 0, \quad \text{at } z = 0 \text{ and } H. \quad (21)$$

Differentiating  $\tilde{\Theta}_0$  and applying the limiting form of the Bessel function for small argument, that is,

$$I_\nu(\phi) \rightarrow (\frac{1}{2}\phi)^\nu / \Gamma(1+\nu), \quad \text{as } \phi \rightarrow 0, \quad (22)$$

where  $\Gamma$  is the gamma function, yields the solution that satisfies the boundary condition at  $z = 0$ , namely

$$\tilde{\Theta}_{01}(z, w) = B_1 z^{\frac{1}{2}m} I_{-\nu}(\phi), \quad (23)$$

for  $0 \leq z < z_0$  and  $B_1$  a constant.

Next the boundary condition at  $z = H$  must be considered. Differentiating equation (19) and setting the resultant expression, evaluated at  $z = H$ , equal to zero gives the solution that satisfies the boundary condition at the surface. This is given by

$$\tilde{\Theta}_{02}(z, w) = B_2 z^{\frac{1}{2}m} \{I_{\nu-1}(\phi_H) I_{-\nu}(\phi) - I_{1-\nu}(\phi_H) I_{\nu}(\phi)\}, \quad (24)$$

for  $z_0 < z \leq H$  and  $B_2$  a constant, and

$$\phi_H = (w/b)^{\frac{1}{2}} 2H^{\frac{1}{2}(1+m)} / (1+m) = hw^{\frac{1}{2}}. \quad (25)$$

The constants  $B_1$  and  $B_2$  are determined by matching the two solutions  $\tilde{\Theta}_{01}$  and  $\tilde{\Theta}_{02}$  at  $z = z_0$ . The continuity and jump conditions given in equations (17b) and (17c) yield the following set of linear algebraic equations in the unknowns  $B_1$  and  $B_2$ :

$$B_1 \tilde{\Theta}_{01}(z_0) - B_2 \tilde{\Theta}_{02}(z_0) = 0, \quad -B_1 \frac{d\tilde{\Theta}_{01}}{dz} + B_2 \frac{d\tilde{\Theta}_{02}}{dz} = \frac{M}{bz_0^{1-m}}. \quad (26a, b)$$

These equations have a unique solution if and only if the determinant of the coefficients is nonzero. In fact this determinant is the Wronskian of  $\tilde{\Theta}_{01}$  and  $\tilde{\Theta}_{02}$  evaluated at  $z_0$ , and since the two solutions are independent their Wronskian cannot vanish. Thus equations (26) can be solved to give

$$B_1 = \Gamma \{ [I_{\nu-1}(\phi_H) I_{-\nu}(\phi_{z_0}) - I_{1-\nu}(\phi_H) I_{\nu}(\phi_{z_0})] / I_{1-\nu}(\phi_H) \}, \quad (27a)$$

$$B_2 = \Gamma I_{-\nu}(\phi_{z_0}) / I_{1-\nu}(\phi_H), \quad (27b)$$

where

$$\Gamma = \frac{M\pi z_0^{\frac{1}{2}m}}{b(1+m)\sin\nu\pi}, \quad \phi_{z_0} = \frac{(w/b)^{\frac{1}{2}} 2z_0^{\frac{1}{2}(1+m)}}{1+m} = lw^{\frac{1}{2}}. \quad (28a, b)$$

Thus the final solution for  $\tilde{\Theta}_0(z, w)$  becomes

$$\tilde{\Theta}_0(z, w) = B_1 z^{\frac{1}{2}m} I_{-\nu}(\phi), \quad 0 \leq z < z_0 \quad (29a)$$

$$= B_2 z^{\frac{1}{2}m} \{I_{\nu-1}(\phi_H) I_{-\nu}(\phi) - I_{1-\nu}(\phi_H) I_{\nu}(\phi)\}, \quad z_0 < z \leq H. \quad (29b)$$

The inversion theorem for the Laplace transform states that

$$\Theta_0(z, t) = \frac{1}{2\pi i} \int_{\gamma-i\infty}^{\gamma+i\infty} \exp(wt) \tilde{\Theta}_0(z, w) dw, \quad \text{for } t > 0, \quad (30)$$

where  $\gamma$  is such that all singularities of  $\tilde{\Theta}_0$  lie to the left of the line  $(\gamma - i\infty, \gamma + i\infty)$ . The inversion integral is now evaluated for the two domains for which  $\tilde{\Theta}_0(z, w)$  is defined.

*Domain*  $0 \leq z < z_0$

Substituting for  $\tilde{\Theta}_0$  from equations (29) in equation (30) gives

$$\Theta_0(z, t) = \frac{\Gamma z^{\frac{1}{2}m}}{2\pi i} \int_{\gamma-i\infty}^{\gamma+i\infty} \exp(wt) \frac{I_{-\nu}(\phi)}{I_{1-\nu}(\phi_H)} \{I_{-\nu}(\phi_{z_0}) I_{\nu-1}(\phi_H) - I_{\nu}(\phi_{z_0}) I_{1-\nu}(\phi_H)\} dw, \quad (31)$$

with  $\phi_H = hw^{\frac{1}{2}}$ ,  $\phi_{z_0} = lw^{\frac{1}{2}}$  and  $\phi = kw^{\frac{1}{2}}$ , where  $h$ ,  $k$  and  $l$  are constants. The integrand in equation (31) can be shown to be a single-valued function of  $w$  (Watson

1958). It has simple poles at  $w = 0$  and  $-\alpha_n^2/h^2$ , where  $\pm\alpha_n$ ,  $n = 1, 2, \dots$ , are the zeros, all real and simple, of  $J_{1-\nu}(\alpha) = 0$ , where  $J_\nu$  is the Bessel function of the first kind of order  $\nu$ . Since  $\nu$  is real, the zeros of  $J_\nu$  are symmetric with respect to the coordinate axes (Erdélyi *et al.* 1953). Hence only the positive values of  $\alpha_n$  will be considered.

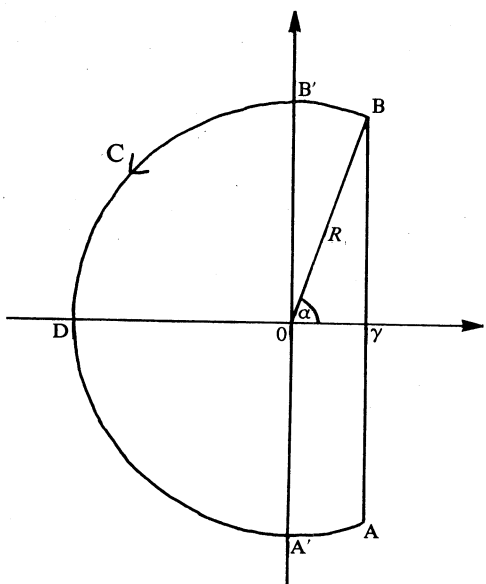


Fig. 2. Contour C used in evaluation of the integral in equation (31).

In order to evaluate the contour integral in equation (31) the procedure outlined in Carslaw and Jaeger (1959) is adopted. The contour is completed by a large circle C of radius R (see Fig. 2) such that no pole of the integrand lies on C. From the theory of Bessel functions of order in the range  $\frac{1}{2}$  to  $\frac{5}{2}$  (Watson 1958), the only positive zeros of  $J_{1-\nu}(\alpha)$  lie in the intervals  $\{m\pi + \frac{1}{4}(\frac{1}{2} - \nu)\pi, m\pi + \frac{1}{2}(\frac{1}{2} - \nu)\pi\}$ , with  $0 < \nu < \frac{1}{2}$  and  $m = 0, 1, 2, \dots$ . Hence if R is set equal to  $m^2\pi^2/h^2$  then no pole of the integrand lies on C.

Since the integrand is regular on C and in the whole  $w$ -plane except for simple poles on the real axis, then Cauchy's Residue Theorem is applicable. Thus, from Fig. 2 we have

$$\int_C \exp(wt) \tilde{\Theta}_0(z, w) dw = \int_{AB} \exp(wt) \tilde{\Theta}_0(z, w) dw + \int_{BDA} \exp(wt) \tilde{\Theta}_0(z, w) dw. \quad (32)$$

When R tends to infinity the integral over the arc BDA tends to zero, and thus

$$\Theta_0(z, t) = \frac{\Gamma}{2\pi i} z^{\frac{1}{2}m} \lim_{R \rightarrow \infty} \int_{AB} F(w) dw = \Gamma z^{\frac{1}{2}m} \sum_p^{\infty} \text{res}\{F(w), w_p\}. \quad (33)$$

If we evaluate the residues at  $w = 0$  and  $-\alpha_n^2/h^2$ , the final solution for the zeroth moment in the domain  $0 \leq z < z_0$  becomes

$$\begin{aligned} \Theta_0(z, t) = & \frac{M}{H} + \frac{M(1+m)}{H^{1+m}} (zz_0)^{\frac{1}{2}m} \sum_{p=1}^{\infty} \exp(-t\alpha_p^2/h^2) J_{-\nu}\{(z/H)^{\frac{1}{2}(1+m)} \alpha_p\} \\ & \times J_{-\nu}\{(z_0/H)^{\frac{1}{2}(1+m)} \alpha_p\} / \{J_{-\nu}(\alpha_p)\}^2. \end{aligned} \quad (34)$$

Domain  $z_0 < z \leq H$

The analysis proceeds exactly as above and since the first term of the integrand in this case is identical to the first term in  $F(w)$  above, and the contribution from the second term is identically zero, the evaluation of the residues yields the same final solution for  $\Theta_0(z, t)$ .

Hence the solution given in equation (34) in fact holds over the entire  $z$  domain, that is for  $0 \leq z \leq H$ . The solution has the correct asymptotic behaviour in that as  $t$  tends to infinity the second term in equation (34) tends to zero. Thus we have

$$\lim_{t \rightarrow \infty} \Theta_0(z, t) = M/H, \quad (35)$$

which states that the tracer is uniformly distributed over the depth at large times. The factor  $h^2$  in equation (34) has dimensions of time and may be interpreted as the vertical mixing time  $T_m$ . From equation (25)  $h^2$  is given by

$$h^2 = T_m = 4H^{1+m}/b(1+m)^2. \quad (36)$$

#### 4. Solution for First Moment

Equation (7) may be re-written as

$$\frac{\partial \Theta_1}{\partial t} - \frac{\partial}{\partial z} \left( K_{zz}(z) \frac{\partial \Theta_1}{\partial z} \right) = q(z, t), \quad (37)$$

where  $q(z, t) = u(z) \Theta_0(z, t)$  is considered to be a source term. The conditions to be satisfied by  $\Theta_1(z, t)$  are given in equations (9). Applying Green's theorem to equation (37) and using the boundary conditions gives

$$\Theta_1(z, t) = \int_0^t \int_0^H G(z, t; z', t') q(z', t') dz' dt', \quad (38)$$

where  $G(z, t; z', t')$  is the causal Green function which can be shown to satisfy the boundary value problem

$$\frac{\partial G}{\partial t} - \frac{\partial}{\partial z} \left( K_{zz} \frac{\partial G}{\partial z} \right) = \delta(z-z') \delta(t-t'), \quad -\infty < t, t' < \infty, \quad 0 < z, z' < H; \quad (39a)$$

$$G(z, t; z', t') \equiv 0, \quad t < t'; \quad K_{zz} \partial G / \partial z = 0, \quad \text{at } z = 0 \text{ and } H. \quad (39b, c)$$

Now the Green function for  $t > t'$  can equally well be characterized as the solution of the following problem (Stakgold 1968):

$$\frac{\partial G}{\partial t} - \frac{\partial}{\partial z} \left( K_{zz} \frac{\partial G}{\partial z} \right) = 0; \quad (40a)$$

$$\lim_{t \rightarrow t'} G(z, t; z', t') = \delta(z-z'); \quad K_{zz} \partial G / \partial z = 0, \quad \text{at } z = 0 \text{ and } H. \quad (40b, c)$$

By comparison with the problem for  $\Theta_0(z, t)$  given in equations (5) and (6) the Green function may be shown to be given by

$$G(z, t; z', t') = M^{-1} \Theta_0(z, t-t'), \quad \text{for } t > t'. \quad (41)$$

Substituting into equation (38) gives

$$\Theta_1(z, t) = M^{-1} \int_0^t \int_0^H \Theta_0(z, t-t') q(z', t') dz' dt'. \quad (42)$$

Carrying out the integrations indicated and simplifying yields the expression for the first moment

$$\begin{aligned} \Theta_1(z, t) = & \frac{MH^{m-1}at}{1+m} + 4MH^{\frac{1}{2}(m-2)}az^{\frac{1}{2}m} \sum_{p=1}^{\infty} \left[ \left\{ \left( \frac{2^v}{\Gamma(-v)} + v\alpha_p^v J_{-v}(\alpha_p) \right) / \alpha_p^{v+2} \right\} \right. \\ & \times \frac{J_{-v}\{(z_0/H)^{\frac{1}{2}(1+m)}\alpha_p\}}{\{J_{-v}(\alpha_p)\}^2} \frac{h^2}{\alpha_p^2} \left( 1 - \exp(-t\alpha_p^2/h^2) \right) \left. \right] \\ & + 4MH^{\frac{1}{2}(m-2)}az^{\frac{1}{2}m} \sum_{p=1}^{\infty} \left[ \left\{ \left( \frac{2^v}{\Gamma(-v)} + v\alpha_p^v J_{-v}(\alpha_p) \right) / \alpha_p^{v+2} \right\} \right. \\ & \times \frac{J_{-v}\{(z/H)^{\frac{1}{2}(1+m)}\alpha_p\}}{\{J_{-v}(\alpha_p)\}^2} \frac{h^2}{\alpha_p^2} \left( 1 - \exp(-t\alpha_p^2/h^2) \right) \left. \right] \\ & + \frac{M}{H} 2(1+m)a(zz_0)^{\frac{1}{2}m} \sum_{n=1}^{\infty} \sum_{p=1}^{\infty} \left\{ J_{-v}\{(z/H)^{\frac{1}{2}(1+m)}\alpha_n\} \right. \\ & \times \frac{J_{-v}\{(z_0/H)^{\frac{1}{2}(1+m)}\alpha_p\}}{\{J_{-v}(\alpha_n)J_{-v}(\alpha_p)\}^2} \left( \delta_{np} t \exp(-t\alpha_n^2/h^2) + \frac{h^2}{\alpha_n^2 - \alpha_p^2} \right. \\ & \times (1 - \delta_{np}) \{ \exp(-t\alpha_p^2/h^2) - \exp(-t\alpha_n^2/h^2) \} \left. \right) \\ & \times \int_0^1 dk k^{2v+1} J_{-v}(k\alpha_n) J_{-v}(k\alpha_p) \left. \right\}, \quad (43) \end{aligned}$$

where  $\delta_{np}$  is the Kronecker delta. The integrals over  $k$  in the last term could not be evaluated analytically; they were however computed numerically using a Gauss 16 point quadrature.

The asymptotic behaviour of the centroid of the patch can now be deduced from equation (8). Substituting for the first and zeroth moments evaluated at large times gives

$$\bar{x}(z, t \rightarrow \infty) = H^m at / (m+1) + C, \quad (44)$$

where  $C$  is a constant independent of time. Thus the centroid moves asymptotically with the depth mean velocity, which is as expected since the tracer is uniformly distributed over the depth at large times.

## 5. Statistics of Entire Patch

Integrating equation (7) over the depth and applying the boundary conditions gives

$$\frac{\partial \Phi_1}{\partial t} = \int_0^H u(z) \Theta_0(z, t) dz. \quad (45)$$

Integrating over  $z$  and  $t$  yields the expression for the depth integrated first moment

$$\begin{aligned} \Phi_1(t) = & \frac{MH^m at}{1+m} + 4Ma(Hz_0)^{\frac{1}{2}m} \sum_{n=1}^{\infty} \left[ \left\{ \left( \frac{2^v}{\Gamma(-v)} + v\alpha_n^v J_{-v}(\alpha_n) \right) / \alpha_n^{v+2} \right\} \right. \\ & \times \left. \frac{J_{-v}\{(z_0/H)^{\frac{1}{2}(1+m)}\alpha_n\}}{\{J_{-v}(\alpha_n)\}^2} \frac{h^2}{\alpha_n^2} \left( 1 - \exp(-\alpha_n^2 t/h^2) \right) \right]. \end{aligned} \quad (46)$$

The centroid of the entire patch is given by equation (13) with  $\Phi_1(t)$  as above. It is noted that this result could have also been derived by integrating the expression for the first moment given in equation (43) over the depth.

The depth integrated second moment can be derived from equation (10) by integrating with respect to  $z$  to give

$$\frac{\partial \Phi_2}{\partial t} = 2 \int_0^H \{K_{xx} \Theta_0(z, t) + u(z) \Theta_1(z, t)\} dz.$$

Since the contribution of longitudinal diffusion to the variance will be small compared with that of shear diffusion, the diffusivity  $K_{xx}$  will be modelled for simplicity as a constant independent of  $z$ . Carrying out the integration over  $z$  and then integrating over  $t$  gives

$$\begin{aligned} \Phi_2(t) = & 2K_{xx} Mt + \frac{MH^{2m} a^2 t^2}{(1+m)^2} \\ & + \frac{8MH^{3m/2}}{1+m} a^2 z_0^{\frac{1}{2}m} \sum_{p=1}^{\infty} \left[ \left\{ \left( \frac{2^v}{\Gamma(-v)} + v\alpha_p^v J_{-v}(\alpha_p) \right) / \alpha_p^{v+2} \right\} \right. \\ & \times \left. \frac{J_{-v}\{(z_0/H)^{\frac{1}{2}(1+m)}\alpha_p\}}{\{J_{-v}(\alpha_p)\}^2} K_p \left( t - K_p \{1 - \exp(-t/K_p)\} \right) \right] \\ & + \frac{32MH^{2m}}{1+m} a^2 \sum_{p=1}^{\infty} \left[ \left\{ \left( \frac{2^v}{\Gamma(-v)} + v\alpha_p^v J_{-v}(\alpha_p) \right)^2 / \alpha_p^{2v+4} \right\} \right. \\ & \times \left. \frac{K_p}{\{J_{-v}(\alpha_p)\}^2} \left( t - K_p \{1 - \exp(-t/K_p)\} \right) \right] \\ & + 16MH^{3m/2} a^2 z_0^{\frac{1}{2}m} \sum_{n=1}^{\infty} \sum_{p=1}^{\infty} \left[ \left\{ \left( \frac{2^v}{\Gamma(-v)} + v\alpha_n^v J_{-v}(\alpha_n) \right) / \alpha_n^{v+2} \right\} \right. \\ & \times \left. \frac{J_{-v}\{(z_0/H)^{\frac{1}{2}(1+m)}\alpha_p\}}{\{J_{-v}(\alpha_n) J_{-v}(\alpha_p)\}^2} \left\{ \delta_{np} K_n^2 \{1 - (1+t/K_n) \exp(-t/K_n)\} \right. \right. \\ & \left. \left. + (1 - \delta_{np}) \frac{K_n K_p}{K_p - K_n} \left( K_n \exp(-t/K_n) - K_p \exp(-t/K_p) + K_p - K_n \right) \right\} \right. \\ & \times \left. \int_0^1 dk k^{2v+1} J_{-v}(k\alpha_n) J_{-v}(k\alpha_p) \right], \end{aligned} \quad (47)$$

with  $K_n = h^2/\alpha_n^2$  and  $K_p = h^2/\alpha_p^2$ . The variance of the entire patch is given by equation (14) using this expression for  $\Phi_2(t)$ .

The effective longitudinal diffusivity (also termed the longitudinal dispersion coefficient) is defined as the rate of growth of the variance:

$$K_{\text{eff}} = \frac{1}{2} \frac{d\Sigma_x^2}{dt} = \frac{1}{2M} \left( \frac{d\Phi_2}{dt} - \frac{2\Phi_1}{M} \frac{d\Phi_1}{dt} \right). \quad (48)$$

Substituting for  $\Phi_2$  and  $\Phi_1$  from equations (47) and (46) respectively gives

$$\begin{aligned} K_{\text{eff}} = & K_{xx} + \frac{H^2 m a^2 t}{(1+m)^2} + \frac{4H^{3m/2}}{1+m} a^2 z_0^{\frac{1}{2}m} \sum_{p=1}^{\infty} \left[ \left\{ \left( \frac{2^v}{\Gamma(-v)} + v\alpha_p^v J_{-v}(\alpha_p) \right) / \alpha_p^{v+2} \right\} \right. \\ & \times \frac{J_{-v}\{(z_0/H)^{\frac{1}{2}(1+m)}\alpha_p\}}{\{J_{-v}(\alpha_p)\}^2} K_p \left( 1 - \exp(-t/K_p) \right) \Big] \\ & + \frac{16H^{2m} a^2}{1+m} \sum_{p=1}^{\infty} \left[ \left\{ \left( \frac{2^v}{\Gamma(-v)} + v\alpha_p^v J_{-v}(\alpha_p) \right)^2 / \alpha_p^{2v+4} \right\} \right. \\ & \times \frac{K_p}{\{J_{-v}(\alpha_p)\}^2} \left( 1 - \exp(-t/K_p) \right) \Big] \\ & + 8H^{3m/2} a^2 z_0^{\frac{1}{2}m} \sum_{n=1}^{\infty} \sum_{p=1}^{\infty} \left[ \left\{ \left( \frac{2^v}{\Gamma(-v)} + v\alpha_n^v J_{-v}(\alpha_n) \right) / \alpha_n^{v+2} \right\} \right. \\ & \times \frac{J_{-v}\{(z_0/H)^{\frac{1}{2}(1+m)}\alpha_p\}}{\{J_{-v}(\alpha_n)J_{-v}(\alpha_p)\}^2} \left( \delta_{np} t \exp(-t/K_n) + (1 - \delta_{np}) \frac{K_n K_p}{K_p - K_n} \right. \\ & \times \left. \left. \left\{ \exp(-t/K_p) - \exp(-t/K_n) \right\} \int_0^1 dk k^{2v+1} J_{-v}(k\alpha_n) J_{-v}(k\alpha_p) \right) \right. \\ & - \frac{\Phi_1(t)}{M} \left( \frac{H^m a}{1+m} + 4a(Hz_0)^{\frac{1}{2}m} \sum_{n=1}^{\infty} \left[ \left\{ \left( \frac{2^v}{\Gamma(-v)} + v\alpha_n^v J_{-v}(\alpha_n) \right) / \alpha_n^{v+2} \right\} \right. \right. \\ & \times \left. \left. \frac{J_{-v}\{(z_0/H)^{\frac{1}{2}(1+m)}\alpha_n\}}{\{J_{-v}(\alpha_n)\}^2} \exp(-t/K_n) \right] \right) \Big]. \quad (49) \end{aligned}$$

After substituting again for  $\Phi_1(t)$  from equation (46), the terms that depend on  $t$  linearly cancel, and thus the longitudinal spread of the tracer due to the shear effect is asymptotically governed by a constant effective diffusivity. This result agrees with the conclusions of Okubo (1967).

## 6. Discussion and Illustration of Theoretical Results

For the purposes of illustration the following values are chosen for the constants in the formulae for the velocity and diffusivity profiles:

$$m = 1/7, \quad u^* = 0.006 \text{ m s}^{-1}, \quad u_{av} = 0.3 \text{ m s}^{-1}.$$

With these values the constants  $a$  and  $b$ , defined in equations (1) and (3b), are calculated to be

$$a = 0.25 \text{ m}^{6/7} \text{ s}^{-1}, \quad b = 1.02 \times 10^{-3} \text{ m}^{8/7} \text{ s}^{-1}.$$

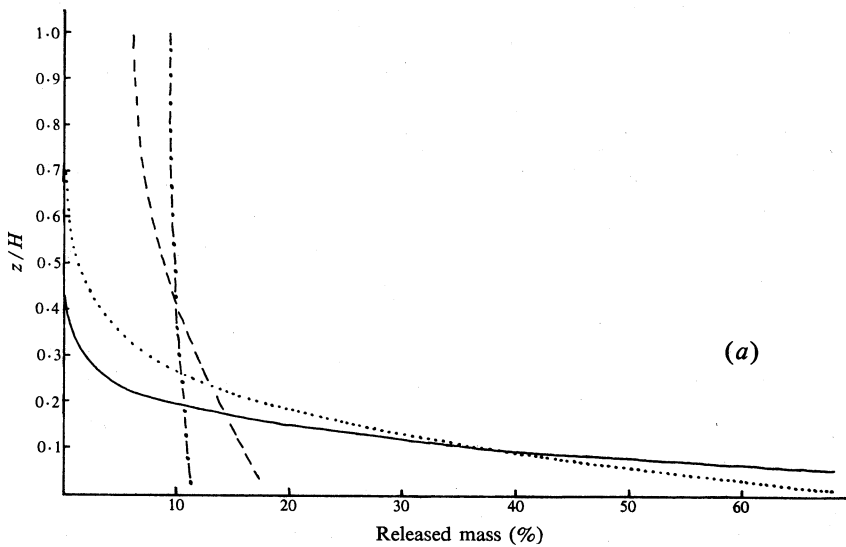


Fig. 3a. (See opposite page)

Hence, the vertical mixing time as defined in equation (36) has the value  $T_m = 3.8 \times 10^4$  s, for a channel of depth 10 m.

The theoretical predictions for the amount of mass that has reached a given depth after a time  $t$  are computed from equation (34). The results are displayed in Fig. 3 for a point source released at  $z_0 = 0.01H$ ,  $0.5H$  and  $H$  respectively. The large velocity gradient in the bottom region of the flow, coupled with the small value of the vertical diffusivity in this region, has a marked effect on vertical mass transport for a release at  $z_0 = 0.01H$ . The model predicts that, at small diffusion times ( $0 < t/T_m < 0.03$ ), almost the entire mass released will be found in the bottom half of the channel, that is,  $0 < z < \frac{1}{2}H$ . In contrast, the rate of vertical mixing of material released at the surface is appreciably greater (see Fig. 3c). A patch released at mid-depth experiences an asymmetric rate of vertical mixing—more mass being transported toward the surface than the bottom. These predictions are consistent with the diffusivity profile, derived by application of Reynolds analogy, and shown in Fig. 1. At large times the approach to a uniform mass distribution over the depth is evident for all three release positions.

The centroid of a patch slice is plotted in Fig. 4 for successive time intervals. The centroid of a patch released at the surface (dashed curves) has been translated further than the centroids of patches released at mid-depth (solid curves) and near the bottom (dotted curves). This is due to the greater flow velocity experienced by material in the upper layers of the channel. The increased difference between the positions of the slice centroids at  $z = H$  and  $0.1H$  at successive time intervals is evidence of the longitudinal spreading of the patch. The difference in the positions of the slice centroids at  $z = H$  and  $0.1H$  is greater for a release at  $z_0 = 0.01H$  than for  $z_0 = H$ , at each time. This implies that greater longitudinal spreading will result for a point release near the bottom than for a release at the surface, and demonstrates the enhanced ability of the lower layer of the flow to disperse material in the streamwise direction. This is confirmed in Fig. 5 where the variance of the

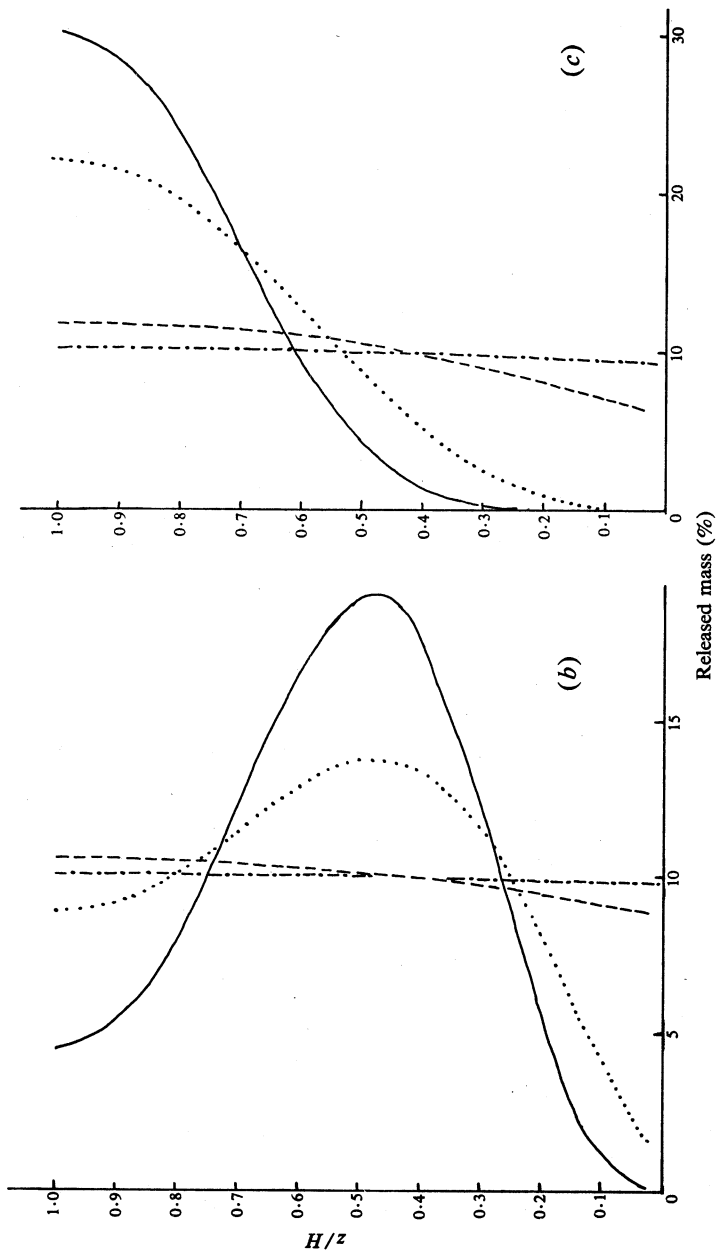
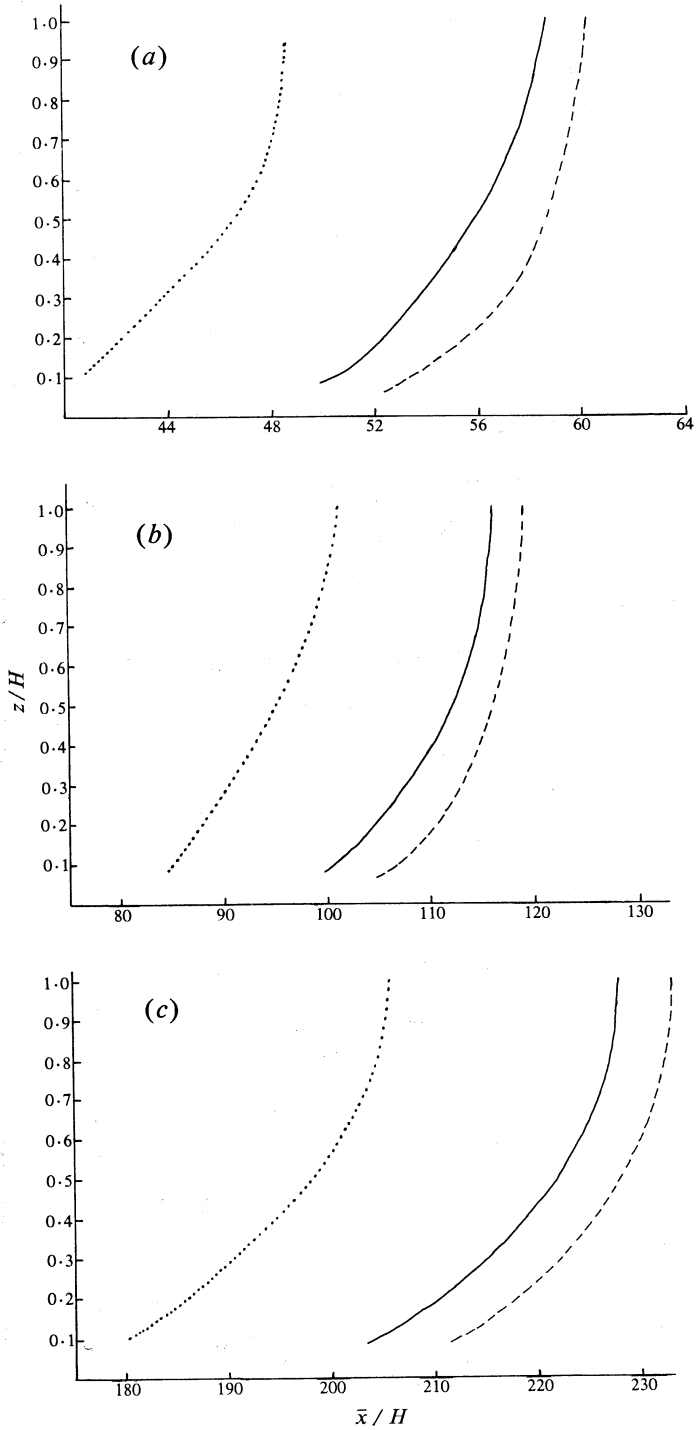


Fig. 3. Mass distribution over depth for source positions (a)  $z_0 = 0.01 H$ , (b)  $z_0 = 0.5 H$  and (c)  $z_0 = H$ . In each case plots are given for four values of the diffusion time  $t/T_m$ : 0.01 (solid curve); 0.03 (dotted curve); 0.10 (dashed curve); 0.30 (dot-dash curve).



**Fig. 4.** Centroids of a patch slice at successive times (a)  $t = 0.05 T_m$ , (b)  $t = 0.1 T_m$  and (c)  $t = 0.19 T_m$ . In each case plots are given for three values of the source positions  $z_0$ :  $0.01 H$  (dotted curve);  $0.5 H$  (solid curve);  $H$  (dashed curve).

entire patch is plotted against diffusion time for the source released at  $z_0 = 0.01 H$ ,  $0.5 H$  and  $H$ . The variance is greatest for a release near the bottom boundary (dotted curve), and least for a release at the surface (dashed curve).

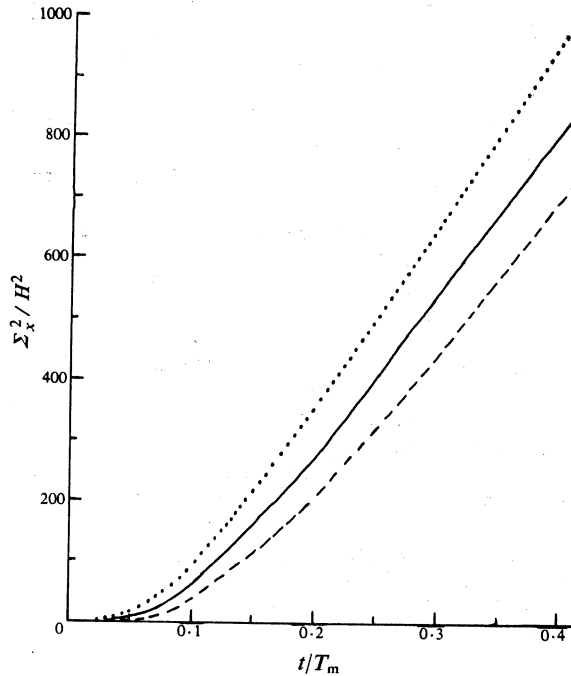


Fig. 5. Variance of entire patch as a function of diffusion time for the three source positions  $z_0 = 0.01 H$  (dotted curve),  $0.5 H$  (solid curve) and  $H$  (dashed curve).

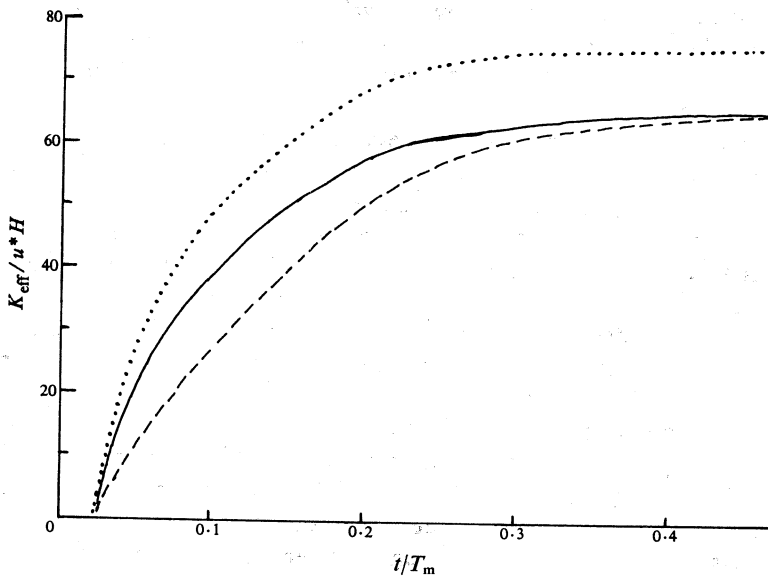


Fig. 6. Effective longitudinal diffusivity as a function of time for the three source positions  $z_0 = 0.01 H$  (dotted curve),  $0.5 H$  (solid curve) and  $H$  (dashed curve).

The variation of the effective longitudinal diffusivity with time is shown in Fig. 6. The magnitude of  $K_{\text{eff}}$  grows rapidly for short times, and then slowly approaches a constant asymptotic value as time increases. The sensitivity to release position is also evident with a release at  $z_0 = 0.01 H$  (dotted curve) being characterized by a greater value of  $K_{\text{eff}}$  than releases at  $z_0 = 0.5 H$  and  $H$ , particularly at short times.

## References

- Aris, R. (1956). *Proc. R. Soc. London A* **235**, 67.  
 Carslaw, H. S., and Jaeger, J. C. (1959). 'Conduction of Heat in Solids', 2nd edn (Oxford Univ. Press).  
 Chatwin, P. C. (1970). *J. Fluid Mech.* **43**, 321.  
 Csanady, G. T. (1973). 'Turbulent Diffusion in the Environment' (Reidel: Dordrecht).  
 Elder, J. W. (1959). *J. Fluid Mech.* **5**, 544.  
 Erdélyi, A., Magnus, W., Oberhettinger, F., and Tricomi, F. G. (1953). 'Higher Transcendental Functions', Vol. 2 (McGraw-Hill: New York).  
 Fukuoka, S. (1973). Res. Bull. Nos C9 and C12, James Cook University of North Queensland.  
 Hinze, J. O. (1959). 'Turbulence: An Introduction to its Mechanism and Theory' (McGraw-Hill: New York).  
 Okubo, A. (1967). *Int. J. Oceanol. Limnol.* **1**, 194.  
 Saffman, P. G. (1962). *Q.J.R. Meteorol. Soc.* **88**, 382.  
 Schubauer, G. B., and Tchen, C. M. (1961). 'Turbulent Flow' (Princeton Univ. Press).  
 Stakgold, I. (1968). 'Boundary Value Problems of Mathematical Physics', Vols 1 and 2 (Macmillan: New York).  
 Sullivan, P. J. (1971). *J. Fluid Mech.* **49**, 551.  
 Taylor, G. I. (1953). *Proc. R. Soc. London A* **219**, 186.  
 Taylor, G. I. (1954). *Proc. R. Soc. London A* **223**, 446.  
 Watson, G. N. (1958). 'A Treatise on the Theory of Bessel Functions', 2nd edn (Cambridge Univ. Press).

## Appendix. Comparison with Experiment

The model's predictions can only be validated by comparison with existing experimental data. Unfortunately no directly relevant field experiments have been conducted. This is probably due to the problems associated with accurate sampling over depth in the field.

Conversely, there are difficulties in measuring concentration profiles over small laboratory flume depths. Consequently, the parameter measured by both Elder (1959) and Sullivan (1971) is the depth-averaged concentration distribution. In addition the experimental techniques employed result in a vertical line source release rather than a point source release. The preceding theory has been developed for a point source because of the relevance to water quality applications. The theoretical results may be integrated over vertical source position to give the equivalent statistics for a line source. Although the algebra becomes cumbersome, this is certainly a possible extension of the theory.

Elder (1959) measured the longitudinal half-width (the longitudinal distance between points at which the dye concentration is half the maximum value) and plotted this parameter against the centroid of the patch at various dispersal times. The results of several realizations were presented and a mean half-width plotted. Elder appears to have assumed the second moment to occur at half the maximum value of the gaussian distribution. Corrected values of the variance derived from the measured half-widths were used in Elder's paper.

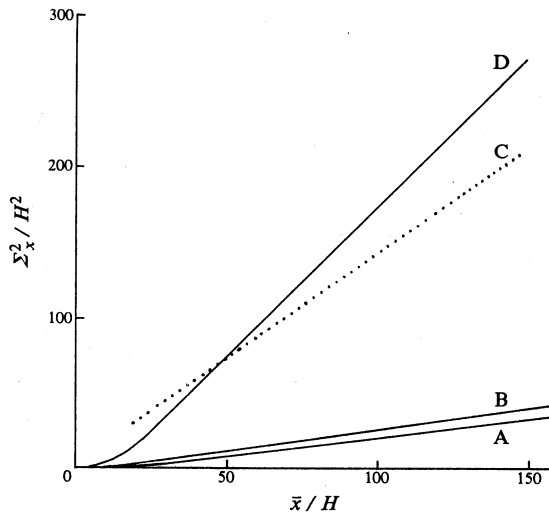


Fig. 7. Patch variance as a function of centroid position for theoretical predictions  $z_0 = H$  (curve A) and  $z_0 = 0.1 H$  (curve B), an approximate line source solution (curve C) and Elder's (1959) experimental results (curve D).

Elder's measurements were made at a Reynolds number of  $R = 3410$  and a depth of  $H = 1.27$  cm. All the mean velocity profiles measured satisfied the logarithmic law and so may be approximated by Prandtl's 1/7th power law. The theoretical results for the variance of a patch released at  $z_0 = H$  and  $0.1 H$  (curves A and B) are shown in Fig. 7 for various centroid positions. The variance for each point source release is less than that measured by Elder for a line source release, as would be expected. An approximate line source solution (curve C) has been derived from the point source solution for comparison with Elder's results (curve D). The predicted patch variance is less than that measured at large diffusion times. This is because the 1/7th law over-estimates the mean fluid velocity near the bottom boundary (Hinze 1959). Otherwise, given the limitations noted above, the predictions compare well with the experimental data. In fact the general structure of the rate of change of the variance is remarkably well reproduced as can be shown by comparing Elder's curves with those of Fig. 5.

